

Context-aware Graph Causality Inference for Few-Shot Molecular Property Prediction

Van Thuy Hoang and O-Joun Lee*

Department of Artificial Intelligence, The Catholic University of Korea
 {hoangvanthuy90, ojlee}@catholic.ac.kr

Abstract

Molecular property prediction is becoming one of the major applications of graph learning in Web-based services, e.g., online protein structure prediction and drug discovery. A key challenge arises in few-shot scenarios, where only a few labeled molecules are available for predicting unseen properties. Recently, several studies have used in-context learning to capture relationships among molecules and properties, but they face two limitations in: (1) exploiting prior knowledge of functional groups that are causally linked to properties and (2) identifying key substructures directly correlated with properties. We propose CaMol, a context-aware graph causality inference framework, to address these challenges by using a causal inference perspective, assuming that each molecule consists of a latent causal structure that determines a specific property. First, we introduce a context graph that encodes chemical knowledge by linking functional groups, molecules, and properties to guide the discovery of causal substructures. Second, we propose a learnable atom masking strategy to disentangle causal substructures from confounding ones. Third, we introduce a distribution intervener that applies backdoor adjustment by combining causal substructures with chemically grounded confounders, disentangling causal effects from real-world chemical variations. Experiments on diverse molecular datasets showed that CaMol achieved superior accuracy and sample efficiency in few-shot tasks, showing its generalizability to unseen properties. Also, the discovered causal substructures were strongly aligned with chemical knowledge about functional groups, supporting the model interpretability.

Introduction

Molecular Property Prediction (MPP) is increasingly being integrated into Web-based platforms, e.g., AlphaFold¹ (Jumper et al. 2021), which provide protein structure prediction online, and drug discovery platforms, e.g., DrugFlow², which recommend candidate molecules for therapeutic properties (Shen et al. 2024; III et al. 2024). In this setting, molecules are represented as graphs, and the task is to predict property labels such as toxicity or solubility from their structural features. However, acquiring labeled molecules remains a challenge, as wet-lab experiments commonly used

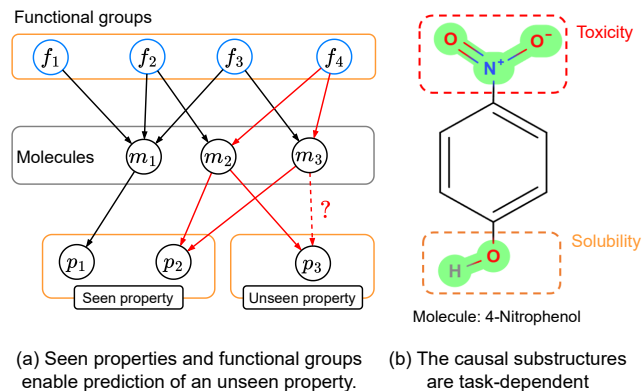


Figure 1: (a) The seen properties are relevant to the unseen property prediction. (b) The causal substructures vary and depend on molecular property prediction tasks.

for annotation are expensive, time-consuming, and prone to human error (III et al. 2024; Liu et al. 2020).

Recently, few-shot learning has emerged as a promising paradigm for solving MPP in data-scarce scenarios (Meng et al. 2023; Liu et al. 2024; Zhuang et al. 2023b; Kim et al. 2019; Guo et al. 2021). Most few-shot MPP approaches adopt a meta-learning framework with episodic training, where models are trained across a distribution of few-shot tasks with the goal of generalizing to unseen properties. These methods can be categorized into two groups: traditional meta-learning approaches and in-context learning approaches. Traditional approaches, e.g., optimization-based (Finn, Abbeel, and Levine 2017; Abbas et al. 2022) and metric-based strategies (Snell, Swersky, and Zemel 2017), focus on acquiring transferable knowledge for rapid adaptation to unseen tasks.

Since many molecular properties are interdependent, recent studies increasingly adopt in-context learning strategies to exploit relationships among molecules and seen properties for predicting unseen properties (Zhuang et al. 2023b; Liu et al. 2024). That is, the model learns the relationship between a few seen molecular examples and properties and then leverages them as contextual signals to predict unseen properties. For example, Pin-Tuning (Liu et al. 2024) builds a context graph to represent molecule–property relationships

*Corresponding author: O-Joun Lee (Tel.: +82-2-2164-5516)

¹<https://alphafold.ebi.ac.uk>

²<https://chem-space.com>

and performs information propagation to derive property-aware molecular representations, improving the prediction of unseen properties.

However, two main challenges limit recent few-shot MPP methods. **(1)** Recent studies mainly focus on relationships between molecules and properties, overlooking the chemical knowledge about functional groups that determine specific properties. As shown in Figure 1(a), only group f_4 serves as the causal substructure responsible for both molecules m_2 and m_3 exhibiting property p_2 , highlighting the insufficiency of modeling at the molecule–property relationship alone. We argue that capturing the interactions among functional groups, molecules, and properties is fundamental for achieving accuracy and interpretability in few-shot MPP tasks. **(2)** It is challenging to identify a key substructure that is directly responsible for a particular property. That is, a single molecule often comprises multiple functional groups, many of which may correlate with different properties. However, for a specific property, only a subset of these substructures, the causal substructure, influences the property, while the remaining substructures are non-informative. As shown in Figure 1(b), consider the molecule 4-nitrophenol ($C_6H_4(NO_2)(OH)$), which contains both a hydroxyl group (OH) and a nitro group (NO_2). The OH group contributes to solubility, whereas the NO_2 group is the key causal determinant of toxicity. Nevertheless, recent methods learn representations by aggregating all substructures, without disentangling key substructures from non-informative parts. As a result, noisy information is incorporated into the graph-level representation, which can hinder the generalization in few-shot scenarios.

To discover important substructures, recent strategies have applied causal inference to graph learning tasks (Sui et al. 2022; Chen et al. 2022). These methods can be grouped into two main categories: intervention-based approaches and invariance-based approaches. The former seeks to mitigate spurious correlations by disentangling causal from non-causal features, while the latter aims to determine stable subgraphs across environments. For example, CAL (Sui et al. 2022) discovers causal patterns and reduces reliance on noisy information by estimating causal and non-causal components with attention modules, applying node-level masking strategies, and backdoor adjustment with noisy interveners. In contrast, GIL (Chen et al. 2022) employs a GNN-based subgraph generator to extract invariant subgraphs while leveraging variant subgraphs to infer environment labels. However, two key challenges remain: **(1)** current methods often overlook relationships among functional groups, which are critical for identifying causal substructures that drive molecular properties and **(2)** most studies rely on random interveners or augmentation-based schemes, which lack semantic grounding and thus fail to provide meaningful guidance for learning causal representations.

In this paper, we assume that each molecule contains a causal substructure that determines its target property, which is context-dependent and influenced by chemical knowledge about functional groups. Unlike previous studies that treat molecules independently, we propose that causal substructures emerge from the relational context linking functional

groups to properties, as shown in Figure 1(a). To achieve this, we construct a context graph that explicitly encodes these multi-level relationships to guide the discovery of causal substructures. Then, we construct a Structural Causal Model (SCM) that identifies the causal substructure C responsible for the target property Y . By using the context graph as contextual signals and integrating graph causality inference, CaMol could estimate the true causal effect of causal substructure C on the target property Y in the few-shot MPP.

Building upon the SCM, we propose CaMol, a novel context-aware graph causality framework for few-shot MPP. CaMol is designed to maximize the causal effect of the discovered causal substructure C on the target property Y by integrating contextual signals and graph causality inference. CaMol is characterized by three main contributions. **(1)** We construct a context graph that encodes the relationships among functional groups, molecules, and properties. This context graph provides contextual guidance for discovering causal substructures, effectively addressing the few-shot challenge of limited labels and chemical priors for causality reasoning. **(2)** We propose a learnable masking mechanism to separate causal substructures C from spurious substructures S . By selectively masking irrelevant atoms, CaMol focuses on key important substructures that are truly responsible for target properties. **(3)** We propose a distribution intervention that parameterizes the backdoor adjustment by pairing causal substructures C with chemically grounded confounders S sampled from remaining molecules. This enables the model to eliminate spurious dependencies and faithfully estimate the causal effect of C on Y . These components allow CaMol to discover interpretable and transferable causal substructures, achieving strong generalization in few-shot MPP tasks.

Related Work

Few-shot Molecular Property Prediction

Traditional few-shot strategies primarily rely on optimization-based and metric-based learning to fine-tune parameter initialization in the latent space (Kim et al. 2019; Alatae-Tran et al. 2016; Vinyals et al. 2016). For example, Meta-MGNN (Guo et al. 2021) improves MAML (Finn, Abbeel, and Levine 2017) with self-attentive task weight meta-learning for few-shot learning. Meta-MGNN incorporates auxiliary self-supervised objectives, such as bond reconstruction and atom type prediction, which are jointly optimized with the MPP tasks to strengthen representation learning. The objective of EGNN (Kim et al. 2019) is to learn the similarity of representations by exploiting intra-cluster similarity and inter-cluster dissimilarity to enhance few-shot performance. However, the traditional methods overlook contextual and causal relations between molecules and properties, which limits their ability to generalize to unseen properties.

Recent strategies have been used in-context learning to guide the prediction of unseen properties by using contextual signals between molecules and properties (Meng et al. 2023; Liu et al. 2024; Zhuang et al. 2023b). These

methods could be systematized into two main groups: molecule–molecule relational modeling and property-aware relational modeling. The first strategies focus on leveraging molecular similarity to improve generalization. PAR (Wang et al. 2021) builds a homogeneous context graph to connect similar molecules and refines embeddings through class prototypes and label propagation. The second line emphasizes molecule–property dependencies to strengthen meta-learning. GS-Meta (Zhuang et al. 2023b) constructs a molecule–property relation graph and redefines episodes as subgraphs of this graph, capturing richer property relations. However, existing methods suffer from two key limitations: they overlook relations of functional groups as causal priors to properties, and they fail to discover key substructures that determine properties.

Causal Inference in Graph Learning

Recent studies have extended causal inference to graph learning, aiming to improve representation quality and robustness for downstream tasks (Yu, Liang, and He 2023; Zhuang et al. 2023a; Chen et al. 2023; Wu et al. 2024; Fang et al. 2024). These strategies fall into two research lines: (i) mitigating spurious correlations via interventions and (ii) discovering invariant causal subgraphs across environments. The former methods primarily focus on mitigating spurious correlations by enforcing robustness against noisy features, while invariant-subgraph methods aim to extract stable causal patterns that generalize across environments. The first line aims to reduce the effect of noisy substructures by applying interventions and enforcing invariance, thereby uncovering stable causal signals. For example, CAL (Sui et al. 2022) disentangles causal from non-causal components using attention, distills causal parts through a node-masking strategy, and applies backdoor adjustment with non-causal interveners. DIR (Fan et al. 2022) similarly enforces robustness by identifying causal subgraphs that remain stable across environments and minimizing interventional risk variance.

In contrast, invariance-based approaches aim to identify subgraphs that remain stable across environments, capturing causal patterns while separating environment-specific variations (Zhuang et al. 2023a; Chen et al. 2022; Li et al. 2022). For example, GIL (Chen et al. 2022) uses a GNN-based subgraph generator to extract invariant subgraphs while using variant ones to infer latent environment labels. The idea of RGCL (Li et al. 2022) is to perform probabilistic sampling over important nodes to highlight causal substructures, while unimportant nodes guide augmentation and align contrastive learning with causal rationale discovery. However, most invariance-based methods ignore contextual signals from functional groups, which are essential for capturing the true causal patterns that determine molecular properties. Moreover, the random or augmented interveners could introduce unrealistic confounding substructures, limiting the reliability of inference across environments.

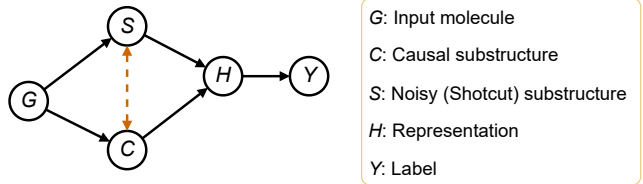


Figure 2: Causal relationships between variables in MPP.

Problem Description

Few-shot Molecular Property Prediction

Let \mathcal{T} be a set of tasks, where each task $T \in \mathcal{T}$ corresponds to predicting a molecular property y . The training set is given by $\mathcal{D}_{\text{train}} = \{(m_i, y_{i,t}) \mid t \in \mathcal{T}_{\text{train}}\}$, while the test set $\mathcal{D}_{\text{test}}$ contains tasks with disjoint property sets, i.e., $\mathcal{P}_{\text{train}} \cap \mathcal{P}_{\text{test}} = \emptyset$.

The goal of few-shot MPP is to learn from $\mathcal{D}_{\text{train}}$ and generalize to unseen tasks in $\mathcal{D}_{\text{test}}$ with only a few labeled molecules. Following standard meta-learning, we adopt episodic training (Finn, Abbeel, and Levine 2017). Typically, the task is formulated as a binary classification, where molecules are labeled as active ($y = 1$) or inactive ($y = 0$). Thus, a 2-way K -shot episode $E_t = (\mathcal{S}_t, \mathcal{Q}_t)$ is constructed, where \mathcal{S}_t refers to the support set, and \mathcal{Q}_t is the query set used for evaluation.

A Causal View in Molecular Graphs

We formalize the causal relationships among the substructures of a molecular graph by using a Structural Causal Model (SCM), as shown in Figure 2. Specifically, we consider the input molecular graph G , which consists of two disjoint substructures: the causal substructure C , which is directly responsible for the molecular property, and the noisy substructure S . We define the SCM as follows, where each link denotes a relationship:

- $C \leftarrow G \rightarrow S$. The input molecular graph G is composed of two disjoint substructures, the causal substructure C and the noisy substructure S .
- $C \rightarrow H \rightarrow Y$. The causal substructure C generates representations H that determine the ground-truth property Y .
- $C \dashrightarrow S$. This denotes a spurious correlation between C and S , which may arise from direct dependence or from unobserved confounders.

Based on our SCM, we identify a backdoor path between C and Y , i.e., $S \leftarrow G \rightarrow C \rightarrow H \rightarrow Y$, where S represents the confounding substructure that introduces spurious correlations between C and Y . To accurately estimate the causal effect of C on Y , it is necessary to block this backdoor path by removing the influence of S , which is the only variable satisfying the backdoor criterion. This ensures that the prediction of Y depends solely on the causal substructure C , rather than on the confounding substructure S . The environmental variable S thus acts as a confounder between G and Y , potentially introducing noisy correlations between C and Y .

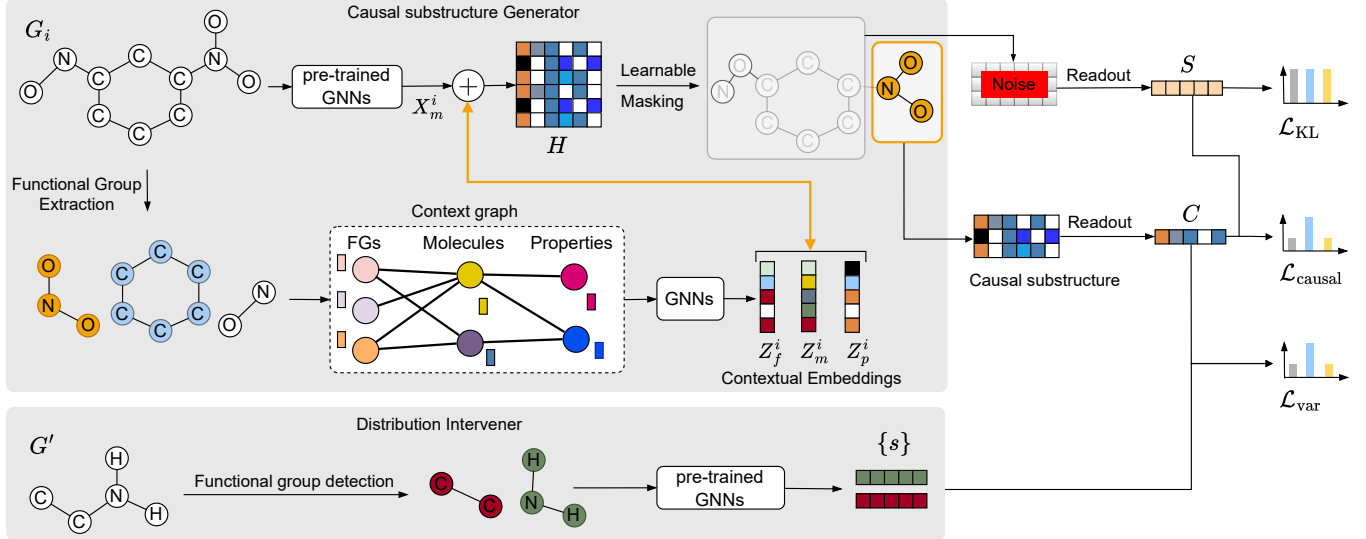


Figure 3: Overview of the CaMol architecture, consisting of a causal substructure extractor and a distribution intervener.

Methodology

Context Graph Learning

To capture the relational structure between molecules and their properties, we construct a context graph that integrates support and query molecule samples within each episode. Specifically, we decompose each molecule into functional groups using the BRICS algorithm (Degen et al. 2008), which uses domain knowledge to fragment molecules into chemically meaningful subgraphs. Given an episode E_t , the context graph is denoted as $G_t = (V_t, A_t, X_t)$. The node set V_t contains three types of nodes: $\{M\}$ molecule nodes, $\{F\}$ functional group nodes, and $\{P\}$ property nodes. Three types of edges are used to represent relationships: positive-label edges, negative-label edges, and unknown-label edges, indicating whether the given molecule is active, inactive, or unknown w.r.t. the property, respectively. This context graph explicitly encodes domain knowledge and relational signals, providing contextual guidance for discovering causal substructures in few-shot MPP. We then learn the node representations with a GNN-based encoder as:

$$Z = \text{GNN}(V_t, A_t, X_t), \quad (1)$$

where $Z \in \mathbb{R}^{(M+F+P) \times d}$ denotes the learned context representation matrix for E_t and $\text{GNN}(\cdot)$ is a GNN encoder, e.g., EGIN (Hu et al. 2020). Here, V_t and A_t denote the node set and adjacency matrix of the context graph, respectively, and X_t denotes the initial features of the nodes. The features of molecules are initialized by the pre-trained molecular encoder S-CGIB (Hoang and Lee 2025), and property nodes are randomly initialized, following the work (Liu et al. 2024).

We note that the context embedding Z contains functional group embeddings Z_f , molecule embeddings Z_m , and property embeddings Z_p . Then, for each input molecule m_i , we obtain its contextual representations by concatenating its representations with the corresponding context embeddings,

as:

$$H_i = (X_m^i \parallel Z_f^i \parallel Z_m^i \parallel Z_p^i), \quad (2)$$

where X_m^i denotes the node-level representation of molecule m_i obtained from the pre-trained encoder S-CGIB, and \parallel denotes vector concatenation. The output node embedding H is then used for causal inference, as represented in the following sections.

Graph Causality Learner for Molecules

Backdoor Adjustment A main challenge in discovering important substructures is the presence of confounding substructures S that correlate spuriously with the label Y , hindering the true causal effect of C . A direct solution would be to collect molecules including C across all possible variations of S from the dataset, but this is infeasible due to the difficulty of acquiring sufficiently diverse and annotated data, especially in few-shot scenarios. Causal theory offers a principled solution via the backdoor adjustment (Wu et al. 2022). Instead of modeling the confounded distribution directly, the model estimates the intervention distribution, as:

$$\begin{aligned} P(Y \mid \text{do}(C)) &= \tilde{P}(Y \mid C) \\ &= \sum_s \tilde{P}(Y \mid C, s) \cdot \tilde{P}(s \mid C) \\ &= \sum_s \tilde{P}(Y \mid C, s) \cdot \tilde{P}(s), \end{aligned}$$

where $\text{do}(C)$ represents an intervention that sets the causal substructure C to a fixed value. Under the assumption that S is independent of C , i.e., $S \perp C$, the intervention distribution $P(Y \mid \text{do}(C))$ can be computed by marginalizing over S using the law of total probability. By doing so, the backdoor adjustment enables the model to make robust and invariant predictions by learning from various confounding substructures. Unlike previous studies, CaMol extends this

idea by (1) refining the intervention space s using semantic substructure confounders that are grounded in chemically meaningful functional groups and (2) incorporating a context graph that encodes prior chemical knowledge to guide the causal inference. The theoretical analysis is provided in Appendix .

Causal Substructure Extractor via Atom Masking To incorporate a causal intervention framework into few-shot MPP, a key challenge is separating the causal substructure C , which directly determines the target property, from confounding substructures S . In molecular graphs, however, this separation is challenging as directly removing substructures could violate chemical validity. To address this, we introduce a learnable masking strategy that disentangles atom-level causal substructures from non-informative ones. Specifically, for each atom v_i , we estimate its relevance to the prediction task with a multilayer perceptron (MLP), as:

$$p_i = \text{MLP}(H_i), \quad (3)$$

where H_i is the atom representation. Based on p_i , we derive atom-level causal and confounding representations through a noise-injected masking scheme, as:

$$C_i = \lambda_i H_i + (1 - \lambda_i) \varepsilon, \quad (4)$$

$$S_i = (1 - \lambda_i) H_i, \quad (5)$$

where $\lambda_i \sim \text{Bernoulli}(p_i)$, $\varepsilon \sim \mathcal{N}(\mu_H, \sigma_H^2)$ is sampled noise, and μ_H and σ_H are the mean and variance of H , respectively. By doing so, the model could disentangle causal substructures by selectively masking unimportant atoms with noisy information with p_i .

To enable differentiable sampling, we adopt the Gumbel-Sigmoid strategy, i.e., $\lambda_i = \text{Sigmoid}(1/\tau \log[p_i/(1-p_i)] + \log[q/(1-q)])$ where $q \sim \text{Uniform}(0, 1)$ and τ is the temperature parameter (Jang, Gu, and Poole 2017; Maddison, Mnih, and Teh 2017). Finally, graph-level embeddings for C and S are obtained via a summation readout function over their node representations.

Distribution Intervention We aim to disentangle causal substructures C whose relationship with the label Y remains invariant despite the presence of noisy confounders S across molecules. To address this, we employ the backdoor adjustment to mitigate the influence of S , which operates implicitly in the representation space. By partitioning the confounders S into distinct groups $S = \{s\}$, we construct multiple s -interventional distributions that help isolate the causal effect of C on the target property Y . The invariance loss can be defined as:

$$\begin{aligned} \mathcal{L}_{\text{var}} &= \sum_{G \in \mathcal{D}_{\text{train}}} \sum_s \mathcal{L}(Y, C, s) \\ &= \sum_{G \in \mathcal{D}_{\text{train}}} \sum_{s \in S} [-y \log \hat{y}_{C,s} - (1 - y) \log(1 - \hat{y}_{C,s})] \end{aligned}$$

where $\hat{y}_{C,s} = f_\theta(C, s)$ denotes the prediction derived from the causal representation C conditioned on the confounder s . Unlike prior studies using augmentation or noise injection, CaMol leverages functional group knowledge to guide interventions. Confounding candidates $\{s\}$ are extracted from functional groups in graphs G' linked to properties different from the target property.

Objective Functions A principle of our framework is that the confounding substructure S carries no predictive information about the label Y . Thus, we regularize the model such that predictions based on S follow a non-informative prior, i.e., a uniform distribution over the label space. Formally, we minimize the KL divergence between the predictive distribution from S and a uniform distribution from the label space, as:

$$\begin{aligned} \mathcal{L}_{\text{KL}} &= \sum_{G \in \mathcal{D}_{\text{train}}} \mathcal{L}(Y_{\text{random}}, S) \\ &= \sum_{G \in \mathcal{D}_{\text{train}}} \text{KL} \left(P_\theta(Y | S) \parallel \mathcal{U}(Y) \right), \end{aligned} \quad (7)$$

where $P_\theta(Y | S)$ is the predicted label distribution from confounding representations and $\mathcal{U}(Y)$ is a uniform distribution.

In contrast, we enforce the causal substructure C to retain predictive information about the label. To achieve this, we optimize a causal prediction loss using cross-entropy:

$$\begin{aligned} \mathcal{L}_{\text{causal}} &= \sum_{G \in \mathcal{D}_{\text{train}}} \mathcal{L}(Y, C) \\ &= \sum_{G \in \mathcal{D}_{\text{train}}} [-y \log \hat{y}_C - (1 - y) \log(1 - \hat{y}_C)] \end{aligned} \quad (8)$$

where $\hat{y}_C = f_\theta(C, S)$ is the prediction based on the causal substructure C and the noise S . The final loss function is defined as:

$$\mathcal{L}_{\text{tot}} = \mathcal{L}_{\text{causal}} + \alpha_1 \mathcal{L}_{\text{KL}} + \alpha_2 \mathcal{L}_{\text{var}}, \quad (9)$$

where α_1 and α_2 are hyperparameters.

Meta-training Optimization

Following the MAML framework (Finn, Abbeel, and Levine 2017), we adopt a gradient-based meta-learning strategy. A batch of B episodes $\{\mathcal{E}_t\}_{t=1}^B$ is randomly sampled. For each episode \mathcal{E}_t , the inner-loop optimization is performed on the support set \mathcal{S}_t by computing the total loss:

$$\mathcal{L}_S(f_\theta) = \frac{1}{B} \sum_{t=1}^B \left(\mathcal{L}_{\text{causal}}^{(t,S)} + \alpha_1 \mathcal{L}_{\text{KL}}^{(t,S)} + \alpha_2 \mathcal{L}_{\text{var}}^{(t,S)} \right), \quad (10)$$

where f_θ denotes the model parameterized by θ . The model parameter θ is then updated via gradient descent:

$$\theta' \leftarrow \theta - \alpha_{\text{inner}} \nabla_\theta \mathcal{L}_S(f_\theta), \quad (11)$$

where α_{inner} is the inner-loop learning rate.

In the outer loop, the model update parameter θ' is evaluated on the corresponding query set \mathcal{Q}_t , and the classification loss is computed as \mathcal{L}_Q . The total meta-training objective across all B tasks incorporates both the query-set causal loss, as:

$$\mathcal{L}_Q(f_{\theta'}) = \frac{1}{B} \sum_{t=1}^B \left(\mathcal{L}_{\text{causal}}^{(t,Q)} + \alpha_1 \mathcal{L}_{\text{KL}}^{(t,Q)} + \alpha_2 \mathcal{L}_{\text{var}}^{(t,Q)} \right), \quad (12)$$

where λ_1 and λ_2 are hyper-parameters. The model parameters are updated using an outer-loop gradient descent step:

$$\theta \leftarrow \theta - \alpha_{\text{outer}} \nabla_\theta \mathcal{L}_Q(f_{\theta'}), \quad (13)$$

where α_{outer} is the meta-learning rate. The training process is provided in Appendix B.

Computational Complexity Analysis

CaMol introduces only a lightweight computational overhead compared to standard few-shot GNN baselines, e.g., MAML (Finn, Abbeel, and Levine 2017). The molecular backbone uses a pre-trained S-CGIB encoder (Hoang and Lee 2025), whose cost is fixed and thus does not increase the training complexity of CaMol. In each episode, the context graph encoder processes N_c nodes and E_c edges with a complexity of $O(L_c(N_c + E_c)d)$, where L_c is the number of GNN layers and d is the embedding dimension. The causal substructure generator consists of two lightweight MLPs applied at the atom level, resulting in a complexity of $O(Nd^2)$, where N is the number of atoms in the molecule. The distribution intervention module combines the causal representation with a chemically grounded confounder in the representation space, introducing only constant-time overhead per molecule. Overall, CaMol follows a MAML-style meta-optimization scheme and has a per-iteration complexity of $O(B(L_c(N_c + E_c)d + Ad^2))$, where B is the number of tasks per batch.

Experiments

We evaluate CaMol on three tasks: few-shot performance, molecule interpretation, and model explainability. The first task analyzes whether the found causal substructures can enhance the predictive performance of few-shot MPP. The second task evaluates whether the found causal substructures are consistent with preserving the similar property. The third task is to evaluate whether the explanations are faithful to the model’s decision.

Experimental Settings

Datasets We evaluate CaMol on six widely used few-shot molecular property prediction datasets from MoleculeNet (Wu et al. 2018), including Tox21, SIDER, MUV, ToxCast, PCBA, and ClinTox. For the model explainability, we used three datasets with ground truth substructure explanations, i.e., Benzene, Alkane Carbonyl, and Fluoride Carbonyl (Chirag et al. 2023). We follow the standard data splits commonly adopted in Few-shot MPP to ensure fair comparison with prior work (Altae-Tran et al. 2016). The dataset statistics are given in Appendix C.

Baselines and Implementation Details We adopt two groups of baselines. (1) Traditional methods include: MAML (Finn, Abbeel, and Levine 2017), Sharp-MAML (Abbas et al. 2022), ProtoNet (Snell, Swersky, and Zemel 2017), EGNN (Kim et al. 2019), and Meta-MGNN (Guo et al. 2021). (2) In-context learning methods include: PAR (Wang et al. 2021), GS-Meta (Zhuang et al. 2023b), TPN (Ma et al. 2020), HSL-RG (Ju et al. 2023), and Pin-Tuning (Liu et al. 2024). For the pre-trained encoder, we adopt S-CGIB (Hoang and Lee 2025) as the backbone encoder. We employ a 3-layer EGIN (Hu et al. 2020) as the context graph encoder. The implementation details and reproducibility are provided in Appendix D. We deliver an open-source implementation of CaMol for the experiment reproductions³.

³<https://github.com/NSLab-CUK/CaMol>

Few-shot Performance Analysis

We conducted few-shot experiments on six molecular property prediction datasets under various few-shot settings, as shown in Table 1. We observed that: (1) CaMol consistently achieved the best performance across all settings, with an average relative improvement of 7.36% over the strongest in-context learning baseline. For example, on Tox21 (10-shot), CaMol reached 92.69% ROC-AUC, outperforming GS-Meta (86.38%) by 6.31%. These results indicate that causal substructure discovery and functional group reasoning provide strong inductive biases for few-shot molecular property prediction. (2) In-context learning methods, e.g., Pin-Tuning, PAR, and GS-Meta, outperformed traditional meta-learning approaches. This indicates the effectiveness of leveraging molecular–property relationships in addressing the few-shot tasks. (3) CaMol showed large gains on datasets with high structural diversity and class imbalance, such as MUV and PCBA. For example, on MUV (1-shot), CaMol achieved 76.79%, compared to 65.62% for PAR, a relative improvement of 17.06%. By exploiting chemical signals, CaMol effectively discovered transferable causal substructures, showing strong generalization to unseen properties and high performance across benchmarks.

Molecule Interpretation Analysis

We now evaluate whether the found causal substructures remain consistent across molecules for predicting similar properties, as shown in Table 3. We use three explainable datasets with ground-truth substructure annotations and three properties from the Tox21 dataset. Specifically, we select the top 50% of nodes with the highest probability scores from CaMol’s masking strategy as explainable nodes. For baselines, we identify the top 50% of nodes with the highest positive saliency values as explainable substructures, following Pope et al. (2019). To measure consistency, we compute the Jensen–Shannon Divergence (JSD) between the found causal substructure embeddings with similar properties. We observed that: (1) CaMol consistently outperformed baselines that do not discover causal substructures during training, e.g., Pin-tuning, GS-Meta, and Meta-MGNN, across explainable datasets. For example, on the BENZENE dataset, CaMol reduced JSD by 32.3% relative to the second-best model, showing that its discovered substructures are more consistent and property-relevant. This implies that CaMol could learn the correct and stable substructures that respond to the given properties. (2) The found causal substructures could also improve prediction on unseen properties in Tox21. For example, on the SR-HSE property, CaMol achieved a 33.4% improvement over baselines, emphasizing that causal substructure discovery provides transferable inductive bias for few-shot generalization. To sum up, CaMol could identify minimal yet sufficient substructures that are consistent and interpretable to similar properties.

Since we use functional groups as prior knowledge to guide the causal substructure discovery, we validate whether the found causal substructures preserve chemical knowledge about functional group relationships. To achieve it, we conducted a heatmap analysis of property–property similarity

Table 1: A performance comparison on few-shot MPP tasks in terms of ROC-AUC scores (%).

Methods	Tox21			SIDER			MUV		
	10-shot	5-shot	1-shot	10-shot	5-shot	1-shot	10-shot	5-shot	1-shot
MAML	79.59 \pm 0.33	77.12 \pm 0.61	75.63 \pm 0.18	70.49 \pm 0.54	70.05 \pm 0.87	68.63 \pm 1.51	68.38 \pm 1.27	66.47 \pm 0.32	65.82 \pm 2.49
Sharp-MAML	75.37 \pm 0.23	75.09 \pm 0.72	74.59 \pm 0.56	71.02 \pm 0.81	70.49 \pm 0.29	68.43 \pm 0.96	65.52 \pm 2.01	65.37 \pm 3.33	65.12 \pm 2.98
ProtoNet	72.99 \pm 0.56	72.04 \pm 2.13	68.22 \pm 0.46	61.34 \pm 1.08	60.88 \pm 1.84	57.41 \pm 0.76	68.92 \pm 1.64	64.86 \pm 2.31	64.81 \pm 1.95
EGNN	80.11 \pm 0.31	76.80 \pm 2.62	75.71 \pm 0.21	71.24 \pm 0.37	69.14 \pm 1.22	66.36 \pm 0.29	68.84 \pm 1.35	66.92 \pm 1.27	62.72 \pm 1.97
Meta-MGNN	83.44 \pm 0.14	83.03 \pm 0.25	82.67 \pm 0.20	77.84 \pm 0.34	76.19 \pm 0.65	74.62 \pm 0.41	68.31 \pm 3.06	67.91 \pm 2.09	66.10 \pm 3.98
PAR	82.13 \pm 0.26	81.92 \pm 0.37	80.02 \pm 0.30	75.15 \pm 0.35	74.01 \pm 0.12	72.33 \pm 0.47	68.08 \pm 2.23	67.37 \pm 1.32	65.62 \pm 3.49
TPN	76.05 \pm 0.24	75.45 \pm 0.95	60.16 \pm 1.18	67.84 \pm 0.95	66.52 \pm 1.28	62.90 \pm 1.38	65.22 \pm 5.82	65.13 \pm 0.23	50.00 \pm 0.51
GS-Meta	86.38 \pm 0.69	84.13 \pm 0.72	79.32 \pm 0.89	83.72 \pm 0.54	83.22 \pm 0.51	82.84 \pm 0.67	67.11 \pm 1.95	64.50 \pm 0.20	64.70 \pm 2.88
HSL-RG	77.51 \pm 0.62	75.89 \pm 1.28	72.04 \pm 0.79	75.84 \pm 1.13	73.07 \pm 0.87	70.15 \pm 0.83	69.44 \pm 1.09	68.36 \pm 0.46	66.62 \pm 0.59
Pin-tuning	84.94 \pm 0.35	84.89 \pm 1.08	80.76 \pm 0.43	89.58 \pm 0.58	83.15 \pm 0.24	81.63 \pm 0.81	72.49 \pm 0.21	71.78 \pm 0.24	63.54 \pm 0.77
CaMol (Ours)	92.69\pm0.49	86.89\pm0.62	83.67\pm0.38	91.89\pm0.66	88.43\pm0.74	83.36\pm0.32	84.76\pm0.63	81.37\pm0.74	76.79\pm0.42
Methods	ToxCast			PCBA			ClinTox		
	10-shot	5-shot	1-shot	10-shot	5-shot	1-shot	10-shot	5-shot	1-shot
MAML	68.40 \pm 1.02	67.55 \pm 0.65	61.11 \pm 1.36	66.22 \pm 1.31	65.25 \pm 0.75	62.04 \pm 1.73	74.09 \pm 2.06	72.34 \pm 1.81	71.61 \pm 1.24
Sharp-MAML	66.95 \pm 1.42	65.41 \pm 0.95	63.76 \pm 1.06	73.19 \pm 2.37	71.25 \pm 1.84	69.23 \pm 1.36	77.52 \pm 2.74	76.13 \pm 2.66	74.47 \pm 1.81
ProtoNet	68.87 \pm 0.82	66.25 \pm 1.04	58.55 \pm 1.18	64.93 \pm 1.94	62.29 \pm 2.12	55.79 \pm 1.45	76.83 \pm 1.81	76.11 \pm 1.28	75.42 \pm 0.86
EGNN	66.42 \pm 0.77	65.01 \pm 0.94	63.98 \pm 1.20	69.92 \pm 1.85	68.35 \pm 1.52	67.71 \pm 3.67	74.46 \pm 2.84	74.08 \pm 3.17	73.24 \pm 1.66
Meta-MGNN	76.27 \pm 0.57	75.26 \pm 0.93	72.43 \pm 0.85	72.58 \pm 0.34	72.55 \pm 0.19	72.51 \pm 0.52	79.08 \pm 2.74	77.81 \pm 1.64	76.29 \pm 2.73
PAR	74.77 \pm 0.85	71.25 \pm 1.17	69.45 \pm 1.34	78.35 \pm 2.03	76.15 \pm 1.19	74.02 \pm 1.68	85.41 \pm 2.04	85.12 \pm 1.67	82.68 \pm 1.15
TPN	69.47 \pm 0.71	66.04 \pm 1.14	63.78 \pm 0.05	67.61 \pm 0.33	63.66 \pm 1.64	60.28 \pm 1.39	75.36 \pm 3.09	74.25 \pm 4.02	74.02 \pm 3.27
GS-Meta	72.58 \pm 0.34	72.55 \pm 0.19	72.51 \pm 0.52	79.08 \pm 2.74	77.81 \pm 1.64	76.29 \pm 2.73	81.02 \pm 2.12	80.78 \pm 1.89	80.03 \pm 4.52
HSL-RG	71.34 \pm 1.39	70.57 \pm 0.32	69.81 \pm 0.66	80.21 \pm 0.97	79.07 \pm 0.85	76.69 \pm 0.38	79.22 \pm 1.63	77.03 \pm 1.07	76.61 \pm 0.85
Pin-tuning	84.75 \pm 1.41	83.03 \pm 1.05	76.98 \pm 1.92	80.52 \pm 0.59	78.35 \pm 0.64	75.98 \pm 0.83	89.08 \pm 2.81	87.63 \pm 1.44	83.25 \pm 4.16
CaMol (Ours)	89.64\pm0.25	87.46\pm0.29	82.65\pm0.68	87.74\pm0.59	84.92\pm0.24	78.26\pm0.41	93.83\pm0.85	92.76\pm0.38	89.63\pm0.57

Table 2: A model explainability comparison on functional group detection and few-shot MPP tasks in terms of Fidelity ($Fid-/+$).

Methods	BENZENE		Alkane Carbonyl		Fluoride Carbonyl		SR-HSE		SR-MMP		SR-p53	
	$Fid- \downarrow$	$Fid+ \uparrow$										
MAML	0.322 \pm 0.041	0.625 \pm 0.059	0.329 \pm 0.082	0.561 \pm 0.057	0.373 \pm 0.060	0.571 \pm 0.062	0.364 \pm 0.020	0.545 \pm 0.081	0.331 \pm 0.007	0.589 \pm 0.098	0.386 \pm 0.003	0.562 \pm 0.054
Sharp-MAML	0.348 \pm 0.063	0.585 \pm 0.105	0.318 \pm 0.066	0.594 \pm 0.093	0.415 \pm 0.031	0.606 \pm 0.044	0.382 \pm 0.070	0.592 \pm 0.030	0.260 \pm 0.085	0.605 \pm 0.094	0.370 \pm 0.017	0.551 \pm 0.039
ProtoNet	0.437 \pm 0.075	0.625 \pm 0.091	0.487 \pm 0.054	0.634 \pm 0.090	0.281 \pm 0.049	0.548 \pm 0.071	0.330 \pm 0.066	0.531 \pm 0.021	0.358 \pm 0.090	0.608 \pm 0.003	0.380 \pm 0.075	0.698 \pm 0.021
EGNN	0.388 \pm 0.050	0.616 \pm 0.072	0.397 \pm 0.058	0.520 \pm 0.095	0.318 \pm 0.053	0.681 \pm 0.074	0.405 \pm 0.076	0.676 \pm 0.050	0.367 \pm 0.032	0.616 \pm 0.081	0.311 \pm 0.014	0.654 \pm 0.069
Meta-MGNN	0.329 \pm 0.048	0.672 \pm 0.086	0.365 \pm 0.051	0.571 \pm 0.095	0.446 \pm 0.049	0.672 \pm 0.076	0.420 \pm 0.056	0.475 \pm 0.088	0.387 \pm 0.068	0.639 \pm 0.047	0.325 \pm 0.016	0.620 \pm 0.063
PAR	0.241 \pm 0.071	0.682 \pm 0.051	0.415 \pm 0.054	0.681 \pm 0.072	0.239 \pm 0.063	0.681 \pm 0.077	0.378 \pm 0.043	0.378 \pm 0.043	0.312 \pm 0.008	0.659 \pm 0.025	0.374 \pm 0.004	0.629 \pm 0.067
GS-Meta	0.201 \pm 0.039	0.667 \pm 0.048	0.234 \pm 0.050	0.709 \pm 0.094	0.245 \pm 0.038	0.706 \pm 0.059	0.306 \pm 0.060	0.616 \pm 0.045	0.279 \pm 0.095	0.655 \pm 0.021	0.292 \pm 0.049	0.719\pm0.035
TPN	0.312 \pm 0.071	0.591 \pm 0.065	0.274 \pm 0.048	0.685 \pm 0.063	0.248 \pm 0.085	0.662 \pm 0.078	0.322 \pm 0.025	0.625 \pm 0.033	0.385 \pm 0.053	0.573 \pm 0.038	0.322 \pm 0.062	0.599 \pm 0.015
Pin-Tuning	0.226 \pm 0.041	0.628 \pm 0.072	0.257 \pm 0.073	0.719 \pm 0.093	0.234 \pm 0.031	0.689 \pm 0.072	0.306 \pm 0.027	0.683 \pm 0.031	0.340 \pm 0.064	0.695 \pm 0.096	0.308 \pm 0.055	0.667 \pm 0.085
CaMol (Ours)	0.128\pm0.013	0.741\pm0.060	0.158\pm0.022	0.755\pm0.052	0.144\pm0.013	0.762\pm0.051	0.264\pm0.008	0.697\pm0.063	0.207\pm0.023	0.701\pm0.075	0.203\pm0.052	0.713 \pm 0.088

on six properties in the Tox21, as shown in Figure 5. Specifically, we compared the similarity of substructures derived from CaMol’s causal substructure embeddings with those obtained directly from functional group frequencies. The causal embeddings are then aggregated across molecules for each property, and pairwise similarities are computed using the inverse JSD score, while functional group-based similarities are calculated using the Jaccard score. We observed a strong agreement between the two similarity matrices, with Pearson $r = 0.67$, 95% Confidence Interval [0.61, 0.71] and Spearman $\rho = 0.74$, 95% Confidence Interval [0.70, 0.78], both $p < 0.01$. The heatmap revealed that properties sharing common functional groups cluster together in both spaces, while chemically distinct properties remain well separated. The finding indicates that CaMol effectively captured and preserved prior knowledge even in the few-shot scenarios.

Model Explainability Analysis

To evaluate CaMol’s explainability, we compared its discovered explanations against ground-truth structural annotations (Chirag et al. 2023). We extracted explanations by selecting the top 50% of nodes with the highest probability p , emphasizing the causal substructures most responsible for the prediction. We then used the $Fidelity-/+$ metrics (Amara et al. 2022) to assess how well these explanations aligned with the model’s own predictions, as reported in Table 2. For the baselines, following Pope et al. (2019), we selected the top 50% of nodes with the highest positive saliency values as explanations. We observed that CaMol consistently achieved the best explanation quality on both metrics across all datasets. For example, on BENZENE, CaMol reduced $Fidelity-$ by 36.6% compared to the strongest baseline, showing that its discovered substructures aligned more closely with the model’s own predictions.

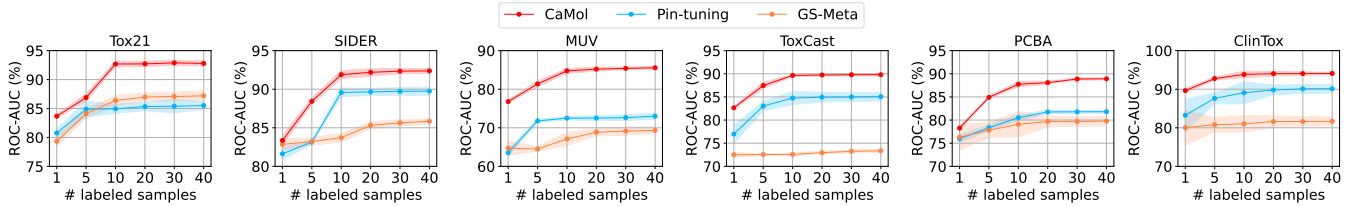


Figure 4: A sample efficiency comparison on Few-shot MPP in terms of ROC-AUC according to the number of labeled samples.

Table 3: A consistency comparison for causal substructures discovered from each property in terms of JSD scores. (BEN.: BENZENE, A.C.: Alkane Carbonyl, F.C.: Fluoride Carbonyl)

Methods	Explainable datasets			Tox21 dataset		
	BEN.	A.C.	F.C.	SR-HSE	SR-MMP	SR-p53
MAML	0.440	0.452	0.502	0.575	0.492	0.470
Sharp-MAML	0.416	0.419	0.478	0.444	0.447	0.437
ProtoNet	0.423	0.431	0.462	0.436	0.481	0.369
EGNN	0.413	0.497	0.437	0.486	0.511	0.391
Meta-MGNN	0.372	0.392	0.503	0.578	0.407	0.343
PAR	0.360	0.492	0.519	0.492	0.353	0.461
GS-Meta	0.318	0.392	0.390	0.308	0.344	0.302
TPN	0.456	0.503	0.494	0.411	0.398	0.326
HSL-RG	0.452	0.684	0.428	0.362	0.331	0.356
Pin-Tuning	0.303	0.414	0.386	0.368	0.287	0.292
CaMol (Ours)	0.205	0.252	0.311	0.205	0.189	0.150

This indicated that CaMol not only improved prediction accuracy but also enhanced interpretability by providing faithful explanations.

Model Efficiency Analysis

We evaluated the generalization and sample efficiency of CaMol across different numbers of labeled molecules, as shown in Figure 4. CaMol consistently demonstrated strong generalization ability and high stability in few-shot scenarios, showing competitive performance even with extremely limited supervision. For example, with only 10 labeled molecules in the Tox21 dataset, CaMol achieved stable high accuracy, showing only marginal improvement as more samples were added. This finding indicated that CaMol effectively learned transferable causal representations that generalized well to unseen properties under data-scarce conditions. We further conducted an efficiency analysis on the trade-off between performance and parameter size (Appendix E.1). We observed that CaMol achieved the best accuracy-efficiency trade-off, positioned on the high-left Pareto frontier.

Ablation Analysis

Model Components To evaluate the contribution of each component in CaMol, we remove the context graph (w/o C.G.), functional groups (w/o F.G.), and the masking strategy (w/o Causality), as shown in Table 4 (a). We observed that: (1) Removing the context graph results in the

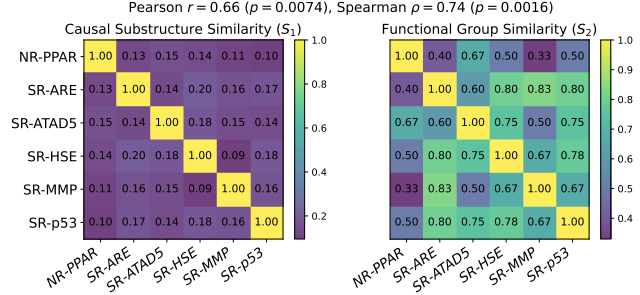


Figure 5: Heatmaps of property–property similarities obtained from (left) representations of causal substructure discovered by CaMol and (right) co-occurrence frequencies of functional groups. The two similarities are highly correlated (Pearson $r = 0.67$, Spearman $\rho = 0.74$; both $p < 0.01$).

largest performance drop across all datasets. For example, on Tox21, performance decreased from 86.89 to 78.66 ROC-AUC, showing that relational signals among molecules, functional groups, and properties are essential for discovering causal substructures. (2) Removing functional groups within the context graph also leads to degradation in performance, e.g., from 88.43 to 86.59 on the SIDER dataset. This implies that functional groups provide an important inductive bias by serving as chemical prior knowledge, which is valuable in few-shot settings. (3) Removing the masking mechanism reduces performance moderately, e.g., from 81.37 to 80.22 on the MUV dataset. Although the impact is smaller compared to the context graph, the consistent decline across datasets implies that masking is important to discover causal substructures, improving prediction on unseen properties. Overall, the context graph delivered relational signals, while graph causal inference focused on key substructures, jointly enabling CaMol’s robust and generalizable performance.

Intervention Strategies We evaluated four intervention strategies: functional group-based (FG-Int, our method), augmentation-based (Aug-Int), random noise (Rand-Int), and no intervention (w/o-Int) under the 5-shot setting, as shown in Table 4 (b). We observed that FG-Int consistently achieved the best and most stable performance across datasets. For example, on Tox21, FG-Int reached 86.89 ROC-AUC, compared to 85.11 for Aug-Int, 86.19 for Rand-Int, and 85.01 without intervention. This implies that interventions grounded in functional groups provided semantic-

Table 4: Ablation study on different components of CaMol, intervention strategies, and loss functions.

	Tox21	SIDER	MUV	ToxCast	PCBA	ClinTox
(a) On different components of CaMol.						
w/o C.G.	78.66	77.7	75.18	79.01	76.21	87.21
w/o F.G.	<u>85.11</u>	<u>86.59</u>	80.14	<u>87.11</u>	<u>84.45</u>	90.35
w/o Causality	<u>84.95</u>	<u>86.15</u>	<u>80.22</u>	86.39	83.49	<u>91.09</u>
CaMol	86.89	88.43	81.37	87.46	84.92	92.76
(b) On different intervention strategies.						
Aug-Int	85.11	87.81	80.95	86.61	<u>84.41</u>	92.51
Rand-Int	<u>86.19</u>	<u>87.94</u>	<u>81.02</u>	<u>87.14</u>	84.22	<u>92.54</u>
w/o-Int	85.01	87.13	79.94	87.03	83.66	91.31
FG-Int (Ours)	86.89	88.43	81.37	87.46	84.92	92.76
(c) On the contribution of different loss functions.						
w/o \mathcal{L}_{KL}	85.01	87.83	79.94	87.03	83.66	91.31
w/o \mathcal{L}_{var}	<u>86.02</u>	<u>87.14</u>	<u>80.78</u>	<u>85.66</u>	82.14	<u>89.35</u>
w/o \mathcal{L}_{causal}	<u>84.95</u>	86.15	<u>80.22</u>	86.39	83.49	91.09
CaMol	86.89	88.43	81.37	87.46	84.92	92.76

cally meaningful priors, allowing the model to disentangle causal substructures more effectively than other interveners.

Loss Functions We further evaluated the contribution of different loss components in CaMol, namely \mathcal{L}_{causal} , \mathcal{L}_{KL} , and \mathcal{L}_{var} , under the 5-shot setting, as shown in Table 4(c). We found that removing any of the loss terms consistently led to a decline in performance compared to CaMol. For example, on Tox21, excluding \mathcal{L}_{causal} caused the large drop, from 86.89 to 84.54 ROC-AUC, underscoring its importance in enforcing causal substructure discovery. Removing \mathcal{L}_{KL} or \mathcal{L}_{var} also reduced performance, indicating that both regularization terms contributed to training stability and generalization. Overall, these results showed that all three objectives worked complementarily to achieve CaMol’s overall performance.

Sensitivity Analysis

We conducted sensitivity analysis by varying causal subgraph ratios and measuring the consistency and model performance under the 5-shot setting (Appendix E.2). We observed that CaMol consistently yielded the lowest JSD at mid-range ratios, from 0.5 to 0.6, which balanced minimal yet sufficient causal substructures and achieved competitive accuracy. Small ratios could discard key atoms, while larger ratios introduced noise, which confirmed CaMol’s robustness in capturing minimal yet consistent causal substructures.

We further analyzed the effect of the hyperparameters α_1 and α_2 , which controlled \mathcal{L}_{KL} and \mathcal{L}_{var} , respectively under the 5-shot setting (Appendix E.3). We observed that CaMol achieved the best performance with moderate values of α_1 and α_2 . That is, the small values weakened the disentanglement and intervention effects, while too large values over-regularized the model. Regarding GNN depth, we observed that CaMol performed best at $k = 3$ layers, as shown in Appendix E.4.

Conclusion

In this paper, we propose CaMol, a novel context-aware causal inference framework for few-shot molecular property prediction. CaMol leverages contextual signals among functional groups and properties to guide causal substructure discovery under the graph causality inference. By integrating a context graph, a learnable masking mechanism, and the chemically grounded interventions, CaMol separates causal substructures from confounding variations. Extensive experiments demonstrated that CaMol consistently outperformed baselines, achieving superior accuracy and sample efficiency in few-shot settings. Moreover, the found causal substructures showed strong alignment with chemical knowledge of functional groups, providing interpretable insights into molecular behavior.

References

- Abbas, M.; Xiao, Q.; Chen, L.; Chen, P.; and Chen, T. 2022. Sharp-MAML: Sharpness-Aware Model-Agnostic Meta Learning. In *Proceedings of the 39th International Conference on Machine Learning (ICML 2022)*, volume 162, 10–32. Baltimore, Maryland, USA: PMLR.
- Altae-Tran, H.; Ramsundar, B.; Pappu, A. S.; and Pande, V. S. 2016. Low Data Drug Discovery with One-shot Learning. arXiv preprint:1611.03199.
- Amara, K.; Ying, Z.; Zhang, Z.; Han, Z.; Zhao, Y.; Shan, Y.; Brandes, U.; Schemm, S.; and Zhang, C. 2022. Graph-FramEx: Towards Systematic Evaluation of Explainability Methods for Graph Neural Networks. In *Proceedings of the 1st Learning on Graphs Conference (LoG 2022)*. Virtual Event.
- Chen, Y.; Bian, Y.; Zhou, K.; Xie, B.; Han, B.; and Cheng, J. 2023. Does Invariant Graph Learning via Environment Augmentation Learn Invariance? In *Proceedings of the 36th Annual Conference on Neural Information Processing Systems (NeurIPS 2023)*. New Orleans, LA, USA.
- Chen, Y.; Zhang, Y.; Bian, Y.; Yang, H.; Ma, K.; Xie, B.; Liu, T.; Han, B.; and Cheng, J. 2022. Learning Causally Invariant Representations for Out-of-Distribution Generalization on Graphs. In *Proceedings of the 35th Annual Conference on Neural Information Processing Systems 2022 (NeurIPS 2022)*. New Orleans, LA, USA.
- Chirag, A.; Owen, Q.; Himabindu, L.; and Marinka, Z. 2023. Evaluating explainability for graph neural networks. *Scientific Data*, 10(1).
- Degen, J.; Wegscheid-Gerlach, C.; Zaliani, A.; and Rarey, M. 2008. On the art of compiling and using ‘drug-like’ chemical fragment spaces. *ChemMedChem*, 3(10): 1503.
- Fan, S.; Wang, X.; Mo, Y.; Shi, C.; and Tang, J. 2022. De-biasing Graph Neural Networks via Learning Disentangled Causal Substructure. In *Proceedings of the 35th Annual Conference on Neural Information Processing Systems 2022 (NeurIPS 2022)*. New Orleans, LA, USA.
- Fang, J.; Li, X.; Sui, Y.; Gao, Y.; Zhang, G.; Wang, K.; Wang, X.; and He, X. 2024. EXGC: Bridging Efficiency and Explainability in Graph Condensation. In *Proceedings*

- of the 33rd ACM on Web Conference 2024 (WWW 2024), 721–732. Singapore: ACM.*
- Fey, M.; and Lenssen, J. E. 2019. Fast Graph Representation Learning with PyTorch Geometric. In *Proceedings of the ICLR Workshop on Representation Learning on Graphs and Manifolds (ICLRW 2019)*.
- Finn, C.; Abbeel, P.; and Levine, S. 2017. Model-Agnostic Meta-Learning for Fast Adaptation of Deep Networks. In *Proceedings of the 34th International Conference on Machine Learning 2017 (ICML 2017)*, volume 70 of *Proceedings of Machine Learning Research*, 1126–1135. Sydney, NSW, Australia: PMLR.
- Guo, Z.; Zhang, C.; Yu, W.; Herr, J.; Wiest, O.; Jiang, M.; and Chawla, N. V. 2021. Few-Shot Graph Learning for Molecular Property Prediction. In *Proceedings of the 30th on The Web Conference 2021 (WWW 2021)*, 2559–2567. Ljubljana, Slovenia: ACM / IW3C2.
- Hoang, V. T.; and Lee, O.-J. 2025. Pre-Training Graph Neural Networks on Molecules by Using Subgraph-Conditioned Graph Information Bottleneck. In *Proceedings of the 39th Conference on Artificial Intelligence (AAAI 2025)*, volume 39, 17204–17213.
- Hu, W.; Liu, B.; Gomes, J.; Zitnik, M.; Liang, P.; Pande, V. S.; and Leskovec, J. 2020. Strategies for Pre-training Graph Neural Networks. In *Proceedings of the 8th International Conference on Learning Representations (ICLR 2020)*. Addis Ababa, Ethiopia: OpenReview.net.
- III, A. R.; Rezaei, M. A.; Friedrich, L.; Buchstaller, H.; Kuhn, D.; and Ghogare, A. 2024. AIDDISON: Empowering Drug Discovery with AI/ML and CADD Tools in a Secure, Web-Based SaaS Platform. *J. Chem. Inf. Model.*, 64(1): 3–8.
- Jang, E.; Gu, S.; and Poole, B. 2017. Categorical Reparameterization with Gumbel-Softmax. In *Proceedings of the 5th International Conference on Learning Representations (ICLR 2017)*. Toulon, France: OpenReview.net.
- Ju, W.; Liu, Z.; Qin, Y.; Feng, B.; Wang, C.; Guo, Z.; Luo, X.; and Zhang, M. 2023. Few-shot Molecular Property Prediction via Hierarchically Structured Learning on Relation Graphs. *Neural Networks*, 163: 122–131.
- Jumper, J.; Evans, R.; Pritzel, A.; Green, T.; Figurnov, M.; Ronneberger, O.; Tunyasuvunakool, K.; Bates, R.; Žídek, A.; Potapenko, A.; et al. 2021. Highly accurate protein structure prediction with AlphaFold. *Nature*, 596(7873): 583–589.
- Kim, J.; Kim, T.; Kim, S.; and Yoo, C. D. 2019. Edge-Labeling Graph Neural Network for Few-Shot Learning. In *Proceedings of the IEEE Conference on Computer Vision and Pattern Recognition 2019 (CVPR 2019)*, 11–20. Long Beach, CA, USA: Computer Vision Foundation / IEEE.
- Li, S.; Wang, X.; Zhang, A.; Wu, Y.; He, X.; and Chua, T. 2022. Let Invariant Rationale Discovery Inspire Graph Contrastive Learning. In *Proceedings of the 34th International Conference on Machine Learning 2022 (ICML 2022)*, volume 162 of *Proceedings of Machine Learning Research*, 13052–13065. Baltimore, Maryland, USA: PMLR.
- Liu, H.; Zhang, W.; Zou, B.; Wang, J.; Deng, Y.; and Deng, L. 2020. DrugCombDB: a comprehensive database of drug combinations toward the discovery of combinatorial therapy. *Nucleic acids research*, 48(D1).
- Liu, Q.; Liu, S.; Sun, X.; Wu, S.; and Wang, L. 2024. Pin-Tuning: Parameter-Efficient In-Context Tuning for Few-Shot Molecular Property Prediction. In *Proceedings of the 38th on Annual Conference on Neural Information Processing Systems 2024 (NeurIPS 2024)*. Vancouver, BC, Canada.
- Ma, Y.; Bai, S.; An, S.; Liu, W.; Liu, A.; Zhen, X.; and Liu, X. 2020. Transductive Relation-Propagation Network for Few-shot Learning. In *Proceedings of the 29th International Joint Conference on Artificial Intelligence 2020 (IJCAI 2020)*, 804–810. ijcai.org.
- Maddison, C. J.; Mnih, A.; and Teh, Y. W. 2017. The Concrete Distribution: A Continuous Relaxation of Discrete Random Variables. In *Proceedings of the 5th International Conference on Learning Representations (ICLR 2017)*. Toulon, France.
- Meng, Z.; Li, Y.; Zhao, P.; Yu, Y.; and King, I. 2023. Meta-Learning with Motif-based Task Augmentation for Few-Shot Molecular Property Prediction. In *Proceedings of the International Conference on Data Mining 2023 (ICDM 2023)*, 811–819. Paul Twin Cities, MN, USA: SIAM.
- Pope, P. E.; Kolouri, S.; Rostami, M.; Martin, C. E.; and Hoffmann, H. 2019. Explainability Methods for Graph Convolutional Neural Networks. In *Proceedings of the IEEE Conference on Computer Vision and Pattern Recognition (CVPR 2019)*, 10772–10781. Long Beach, CA, USA: Computer Vision Foundation / IEEE.
- Shen, C.; Song, J.; Hsieh, C.; Cao, D.; Kang, Y.; Ye, W.; Wu, Z.; Wang, J.; Zhang, O.; Zhang, X.; Zeng, H.; Cai, H.; Chen, Y.; Chen, L.; Luo, H.; Zhao, X.; Jian, T.; Chen, T.; Jiang, D.; Wang, M.; Ye, Q.; Wu, J.; Du, H.; Shi, H.; Deng, Y.; and Hou, T. 2024. DrugFlow: An AI-Driven One-Stop Platform for Innovative Drug Discovery. *J. Chem. Inf. Model.*, 64(14): 5381–5391.
- Snell, J.; Swersky, K.; and Zemel, R. S. 2017. Prototypical Networks for Few-shot Learning. In *Proceedings of the 31st Annual Conference on Neural Information Processing Systems 2017 (NeuIPS 2017)*, 4077–4087. Long Beach, CA, USA.
- Sui, Y.; Wang, X.; Wu, J.; Lin, M.; He, X.; and Chua, T. 2022. Causal Attention for Interpretable and Generalizable Graph Classification. In *Proceedings of the 28th Conference on Knowledge Discovery and Data Mining (KDD 2022)*, 1696–1705. Washington, DC, USA: ACM.
- Vinyals, O.; Blundell, C.; Lillicrap, T.; Kavukcuoglu, K.; and Wierstra, D. 2016. Matching Networks for One Shot Learning. In *Proceedings of the 30th Annual Conference on Neural Information Processing Systems 2016 (NeuIPS 2016)*, 3630–3638. Barcelona, Spain.
- Wang, M.; Zheng, D.; Ye, Z.; Gan, Q.; Li, M.; Song, X.; Zhou, J.; Ma, C.; Yu, L.; Gai, Y.; Xiao, T.; He, T.; Karypis, G.; Li, J.; and Zhang, Z. 2019. Deep Graph Library: A Graph-Centric, Highly-Performant Package for Graph Neural Networks. *arXiv preprint:1909.01315*.

Wang, Y.; Abuduweili, A.; Yao, Q.; and Dou, D. 2021. Property-Aware Relation Networks for Few-Shot Molecular Property Prediction. In *Proceedings of the 35th Annual Conference on Neural Information Processing Systems 2021 (NeurIPS 2021)*, 17441–17454. Virtual Event.

Wu, S.; Cao, K.; Ribeiro, B.; Zou, J. Y.; and Leskovec, J. 2024. GraphMETRO: Mitigating Complex Graph Distribution Shifts via Mixture of Aligned Experts. In *Proceedings of the 38th Annual Conference on Neural Information Processing Systems 2024 (NeurIPS 2024)*. Vancouver, BC, Canada.

Wu, Y.; Wang, X.; Zhang, A.; He, X.; and Chua, T. 2022. Discovering Invariant Rationales for Graph Neural Networks. In *Proceedings of the 10th International Conference on Learning Representations (ICLR 2022)*. Virtual: OpenReview.net.

Wu, Z.; Ramsundar, B.; Feinberg, E. N.; Gomes, J.; Geunesse, C.; Pappu, A. S.; Leswing, K.; and Pande, V. 2018. MoleculeNet: a benchmark for molecular machine learning. *Chemical science*, 9(2).

Xu, K.; Hu, W.; Leskovec, J.; and Jegelka, S. 2019. How Powerful are Graph Neural Networks? In *Proceedings of the 7th International Conference on Learning Representations (ICLR 2019)*. New Orleans, LA, USA: OpenReview.net.

Yu, J.; Liang, J.; and He, R. 2023. Mind the Label Shift of Augmentation-based Graph OOD Generalization. In *Proceedings of Conference on Computer Vision and Pattern Recognition 2023 (CVPR 2023)*, 11620–11630. Vancouver, BC, Canada: IEEE.

Zhuang, X.; Zhang, Q.; Ding, K.; Bian, Y.; Wang, X.; Lv, J.; Chen, H.; and Chen, H. 2023a. Learning Invariant Molecular Representation in Latent Discrete Space. In *Proceedings of the 37th Annual Conference on Neural Information Processing Systems (NeurIPS 2023)*. New Orleans, LA, USA.

Zhuang, X.; Zhang, Q.; Wu, B.; Ding, K.; Fang, Y.; and Chen, H. 2023b. Graph Sampling-based Meta-Learning for Molecular Property Prediction. In *Proceedings of the 32nd International Joint Conference on Artificial Intelligence 2023 (IJCAI 2023)*, 4729–4737. Macao, SAR, China: ijcai.org.

Appendix

A. Theoretical Analysis

We provide a theoretical analysis of CaMol through an information-theoretic lens, e.g., mutual information, to explain how CaMol discovers causal substructures while isolating them from noisy ones. Given an input molecule G , we assume that it contains a causal substructure C that is sufficient for determining its chemical property Y . Formally, this implies that the prediction depends only on the causal component C within G , i.e., $p(Y | G) = p(Y | C, G)$, where p denotes the conditional distribution of the property label Y . We now approximate the true distribution p with a predictive model q from CaMol. To learn this approximation, we minimize the negative conditional log-likelihood of the observed labels. The objective function is defined as:

$$-\mathcal{L} = -\sum_{i=1}^n \log q(Y_i | C_i, G_i), \quad (14)$$

where $q(Y_i | C_i, G_i)$ indicates the probability that the model assigns to the label Y_i given the molecule G_i and its causal substructure C_i . We now decompose this loss as follows:

$$\begin{aligned} -\mathcal{L} &= -\sum_{i=1}^n \log \left[\frac{q(Y_i | C_i)}{p(Y_i | C_i)} \cdot \frac{p(Y_i | C_i)}{p(Y_i | G_i)} \cdot p(Y_i | G_i) \right] \\ &= -\sum_{i=1}^n \left[\log \frac{q(Y_i | C_i)}{p(Y_i | C_i)} + \log \frac{p(Y_i | C_i)}{p(Y_i | G_i)} + \log p(Y_i | G_i) \right] \\ &= \mathbb{E} \left[\log \frac{q(Y_i | C_i)}{p(Y_i | C_i)} \right] + \mathbb{E} \left[\log \frac{p(Y_i | C_i)}{p(Y_i | G_i)} \right] - \mathbb{E} [\log p(Y_i | G_i)] \end{aligned} \quad (15)$$

Then, the second term can be represented as:

$$\begin{aligned} \mathbb{E} \left[\log \frac{p(Y_i | C_i)}{p(Y_i | G_i)} \right] &= \mathbb{E} \left[\log \frac{p(Y_i | C_i)}{p(Y_i | C_i, S_i)} \right] \\ &= \sum_i p(G_i, Y_i) \log \frac{p(Y_i | C_i)}{p(Y_i | C_i, S_i)} \\ &= \sum_i p(G_i, Y_i) \log \left(\frac{p(Y_i | C_i)}{p(Y_i | C_i, S_i)} \cdot \frac{p(S_i | C_i)}{p(S_i | C_i)} \right) \\ &= \sum_i p(G_i, Y_i) \log \frac{p(S_i, Y_i | C_i)}{p(Y_i | C_i) \cdot p(S_i | C_i)} \\ &= I(S; Y | C) \end{aligned} \quad (16)$$

By plugging Equation 16 into Equation 15, we obtain the final objective function, as:

$$\min \mathbb{E} \left[\log \frac{q(Y_i | C_i)}{p(Y_i | C_i)} \right] + I(S; Y | C) + H(Y | G), \quad (17)$$

where the first term denotes the KL divergence between the model distribution q and the true distribution p given causal substructure C , the second term captures the spurious dependence between noise S and labels Y conditioned on C , and the third term denotes the entropy of labels Y given the whole molecule G . Here, our primary interest lies in the second term $I(S; Y | C)$, which measures how much information the confounding substructures S still provide about the labels once the causal substructure C is known. By applying the chain rule, we have:

$$I(S; Y | C) = I(S; Y, C) - I(S; C). \quad (18)$$

This implies that minimizing the second term in Equation 17 encourages the causal substructure C to capture sufficient information about Y . We interpret the behavior of CaMol from two complementary perspectives:

(1) Identifying causal substructures. $I(S; Y | C)$ measures the residual dependence between noisy substructures S and labels Y given the causal substructures C . Minimizing this term ensures that C captures all the information about the label Y , isolating S as redundant. That is, CaMol could disentangle C from S , isolating C as the true substructures that are strongly correlated to Y .

(2) Removing confounding substructures. The residual dependence $I(S; Y)$ quantifies the spurious correlation between noisy substructures S and the target property Y . By minimizing this dependency, CaMol suppresses non-causal signals and prevents the model from treating S as informative for predicting Y , effectively cutting off the direct path $S \rightarrow R \rightarrow Y$ (Figure 2). This ensures that the effect of C on Y is estimated faithfully, aligning predictions with invariant causal mechanisms rather than specific biases.

Algorithm 1: Training process of CaMol

Input: Meta-learning model parameters θ , inner learning rate α_{inner} , meta learning rate α_{outer} , number of tasks per epoch B .

Output: Optimized meta-parameter θ

while not converge **do**

$\mathcal{L}_{\text{total}} \leftarrow 0$

for step = 1 to B **do**

Sample B episode from training set $\mathcal{D}_{\text{train}}$

Compute support loss $\mathcal{L}_S(f_\theta)$ on S by Eq. 10

Compute gradients: $\nabla_\theta \mathcal{L}_S(f_\theta)$

Update: $\theta' \leftarrow \theta - \alpha_{\text{inner}} \nabla_\theta \mathcal{L}_S(f_\theta)$ by Eq. 11

Compute loss $\mathcal{L}_Q(f_{\theta'})$ on query set Q by Eq. 12

$\mathcal{L}_{\text{total}} \leftarrow \mathcal{L}_{\text{total}} + \mathcal{L}_Q(f_{\theta'})$

$\mathcal{L}_{\text{total}} \leftarrow \mathcal{L}_{\text{total}} / B$

Update meta-parameters: $\theta \leftarrow \theta - \alpha_{\text{outer}} \nabla_\theta \mathcal{L}_{\text{total}}$

Return optimized parameter θ .

B. Training Process of CaMol

The training process of CaMol follows a meta-learning paradigm based on episodic optimization, as shown in Algorithm 1. For every task, CaMol initializes task-specific parameters from the shared meta-parameters and performs several inner-loop updates using the support set, guided by the causal substructure generator and distribution intervention. The adapted parameters are then evaluated on the query set, and the resulting query losses are aggregated across tasks to compute the meta-loss. Finally, in the outer-loop optimization, the meta-loss is used to update the global parameters.

C. Statistics of Datasets

We evaluate CaMol on six widely used molecular property prediction benchmarks from MoleculeNet, namely Tox21, SIDER, MUV, ToxCast, PCBA, and ClinTox (Wu et al.

Table 5: An overview of statistics of datasets.

Dataset	Tox21	SIDER	MUV	ToxCast	PCBA	ClinTox
# Compound	7,831	1,427	93,127	8,575	437,929	1,478
# Property	12	27	17	617	128	2
# Train Property	9	21	12	451	118	1
# Test Property	3	6	5	158	10	1
% Label active	6.24	56.76	0.31	12.60	0.84	50.61
% Label inactive	76.71	43.24	15.76	72.43	59.84	49.39
% Missing Label	17.05	0.00	84.21	14.97	39.32	0.00

2018), as shown in Table 5. We follow the standard data splits commonly adopted in Few-shot MPP to ensure fair comparison with prior work (Altae-Tran et al. 2016). In addition, to evaluate the interpretability of CaMol, we further evaluate on three datasets with ground-truth substructure annotations: Benzene, Alkane Carbonyl, and Fluoride Carbonyl (Chirag et al. 2023).

D. Implementation Details

D.1. Model Hyperparameters The detailed hyperparameters of CaMol are provided in Table 6. We train the model with the Adam optimizer, using an initial learning rate of 1×10^{-4} , weight decay of 1×10^{-5} , and a batch size of 8 for 3000 epochs. The context graph encoder is implemented as a 3-layer GIN with edge feature learning (Xu et al. 2019), using an input feature dimension of 64. For graph-level readout, we apply a summation pooling function to aggregate node representations. For meta-learning, the inner-loop and outer-loop learning rates are set to 0.05 and 0.001, respectively.

D.2. Baselines We compare CaMol against two groups of few-shot baselines, including traditional methods and in-context learning methods. For traditional methods, we adopt five approaches:

- **MAML** (Finn, Abbeel, and Levine 2017) is an optimization-based meta-learning framework that learns a shared initialization across tasks.
- **Sharp-MAML** (Abbas et al. 2022) extends MAML by incorporating sharpness-aware minimization during training to better generalize in few-shot adaptation.
- **ProtoNet** (Snell, Swersky, and Zemel 2017) is a metric-based method that represents each class by a prototype in the latent space.
- **EGNN** (Kim et al. 2019) uses edge-aware GNNs to capture relational information about output representations in the latent space.
- **Meta-MGNN** (Guo et al. 2021) uses a meta-learning framework with self-supervised task adaptation to enable effective few-shot MPP tasks.

For in-context learning methods, we adopt five recent methods:

- **PAR** (Wang et al. 2021) presents prototype-based adaptation with relation networks between molecules to improve few-shot MPP.

Table 6: Hyperparameters of CaMol used in experiments.

Hyperparameters	Values
Number of EGIN layers	3
Initial feature dimension	64
Number of training epochs	3000
Adam: initial learning rate	1×10^{-4}
Adam: weight decay	1×10^{-5}
Readout function	SUM
Hyperparameter α_1	0.1
Hyperparameter α_2	0.01
Learning rate in inner-loop α_{inner}	0.05
Learning rate in outer-loop α_{outer}	0.001

- **GS-Meta** (Zhuang et al. 2023b) models inter-task dependencies through exploiting relationships between molecules.
- **TPN** (Ma et al. 2020) uses a context graph to perform label propagation between molecules and properties.
- **HSL-RG** (Ju et al. 2023) employs hierarchical structure learning with relational graphs to capture multi-level contextual information to benefit in-context few-shot adaptation.
- **Pin-Tuning** (Liu et al. 2024) constructs a context graph of molecule and property relationships. By propagating labels through the context graph under learnable adapter layers, it improves adaptability to unseen molecular properties.

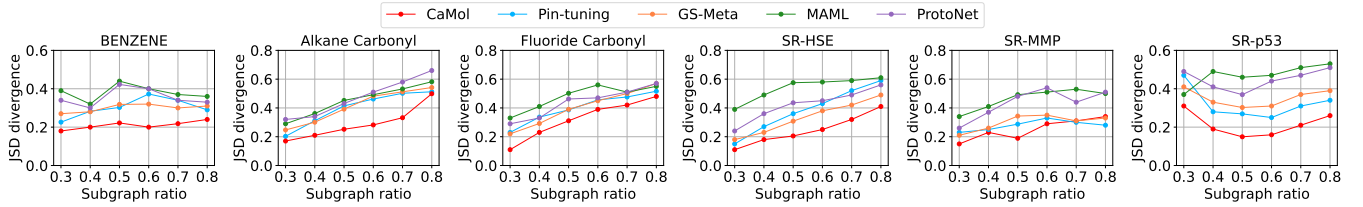
D.3. Training Resources All experiments were run on two servers, each equipped with four NVIDIA RTX A5000 GPUs (24 GB memory per GPU). Our model was implemented in Python 3.8.8, using the PyTorch Geometric framework (Fey and Lenssen 2019) and the DGL (Wang et al. 2019). Experiments were conducted in an Ubuntu 20.04 LTS environment.

D.4. Reproducibility To ensure reproducibility, we release an anonymized implementation of our model, including the full source code and experimental setups, in an open repository⁴.

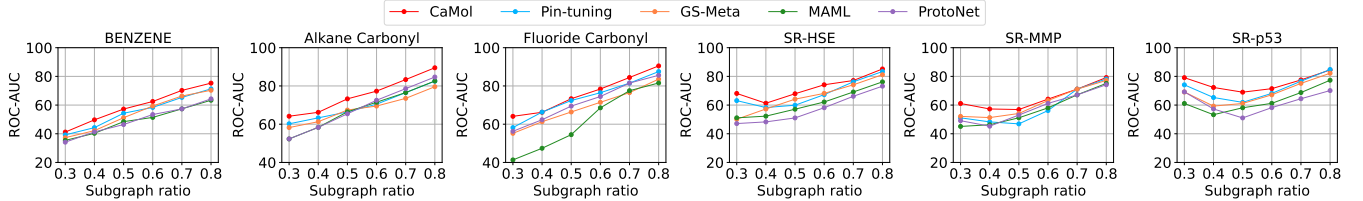
E. Additional Experiments

E.1. Efficiency Analysis of Model Performance versus Parameter Size Figure 7 presents the trade-off between accuracy and parameter size on Tox21, SIDER, and MUV. We observed that CaMol achieved the best accuracy efficiency balance: with only 0.31M parameters, it consistently outperformed in-context methods, e.g., Pin-tuning (1.10M) and GS-Meta (2.66M). This implies that causal substructure discovery provides a stronger inductive bias than simply scaling model size and normal adaptation strategies. In contrast, models with more parameters do not guarantee better accuracy, and traditional meta-learning methods, while parameter-efficient, underperformed significantly. Overall,

⁴<https://anonymous.4open.science/r/CaMol-18A7>



(a) A comparison on consistency of representations of causal substructures according to their sizes (subgraph ratios) in terms of JSD.



(b) A performance comparison on Few-shot MPP according to sizes of discovered causal substructures (subgraph ratios) in terms of ROC-AUC.

Figure 6: Sensitivity comparisons on subgraph ratios in terms of (a) consistency and (b) few-shot performance. Models should discover consistent causal substructures for a property, contributing to prediction accuracy, regardless of substructures sizes.

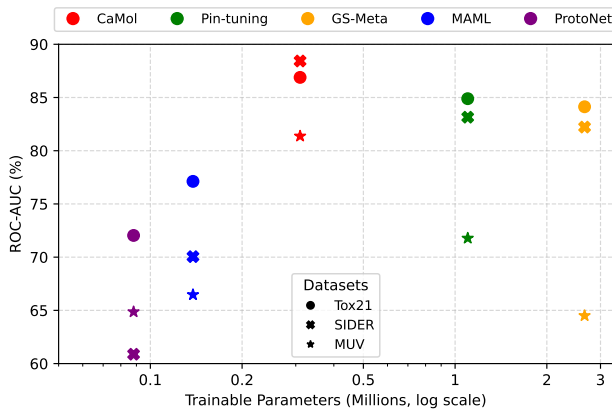


Figure 7: A parameter efficiency comparison on few-shot MPP in terms of ROC-AUC and trainable parameter sizes.

CaMol lies on the Pareto frontier, combining high accuracy with compact parameters.

E.2. Sensitivity Analysis on the Subgraph Ratios We conducted a sensitivity analysis by varying the causal subgraph ratio from 0.3 to 0.8 and evaluating the JSD of the found causal substructures, as shown in Figure 6a. We observed that CaMol consistently achieved the lowest JSD across all ratios, indicating robustness in capturing stable and consistent substructures. The mid-range ratios, i.e., 0.5–0.7, show the best trade-off between sufficiency and performance, indicating that the small ratios attempt to discard important atoms, while very large ratios could introduce noisy signals. These results demonstrate CaMol’s ability to extract minimal yet consistent causal substructures, improving both interpretability and few-shot predictive performance. We further evaluated predictive performance across

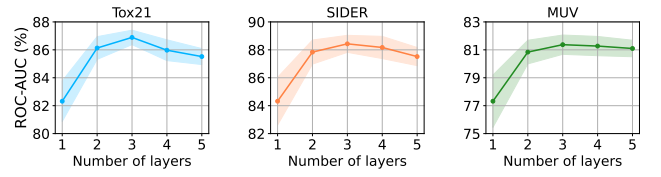
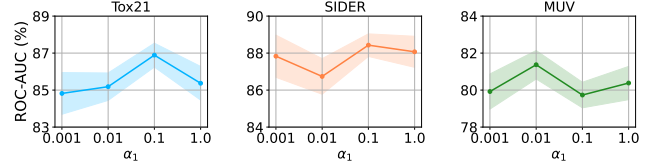
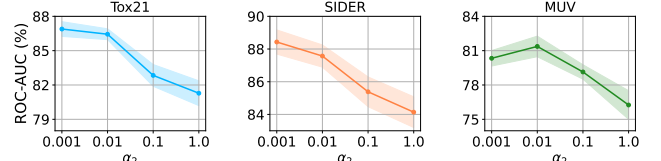


Figure 8: Performance with varying numbers of GNN layers.



(a) Sensitivity analysis on hyperparameter α_1 .



(b) Sensitivity analysis on hyperparameter α_2 .

Figure 9: Sensitivity analysis of the weights in loss function.

six benchmarks, as shown in Figure 6b. Unlike baselines that degrade sharply under small ratios, from 0.3 to 0.5, CaMol maintained competitive accuracy with only marginal losses, demonstrating its robustness in leveraging limited information while scaling effectively with sufficient contexts.

E.3. Sensitivity Analysis of the Weights for Loss Terms We analyze the sensitivity of CaMol to the hyperparamete-

ters α_1 and α_2 , which control the weights of \mathcal{L}_{KL} and \mathcal{L}_{var} , respectively, as shown in Figure 9. For α_1 , CaMol remains stable across a wide range and achieves peak performance at moderate values, e.g., 86.89 ROC-AUC on Tox21. The small values underweight interventions, while overly large ones slightly degrade accuracy. For α_2 , performance is strongest at small values, e.g., 0.001–0.01, but drops at larger ones, e.g., 0.1–1.0, indicating that semantic confounders are helpful but need to be balanced with the context signals.

E.4. Sensitivity Analysis on the Number of Layers We investigated the effect of varying the number of GNN layers on CaMol’s performance across three datasets: Tox21, SIDER, and MUV, as shown in Figure 8. We observed that the model performance is improved as depth increases from 1 to 3 layers, with peak performance observed at 2 or 3 layers, e.g., 86.89 on Tox21 and 88.43 on SIDER. Moreover, additional layers yield marginal or negative gains, suggesting that deeper models introduce over-smoothing without capturing additional useful structure.